The tolerance to hypoxia is defined by a time-sensitive response of the gene regulatory network in sea urchin embryos

Majed Layous, Lama Khalaily, Tsvia Gildor and Smadar Ben-Tabou de-Leon*

Department of Marine Biology, Leon H. Charney School of Marine Sciences, University of Haifa, Haifa 31905, Israel.

*Correspondence: Smadar Ben-Tabou de-Leon (sben-tab@univ.haifa.ac.il)

Abstract

Deoxygenation, the reduction of oxygen level in the oceans induced by global warming and anthropogenic disturbances, is a major threat to marine life. Acute diurnal changes in oxygen levels could be especially harmful to vertebrate and sea urchin embryos that utilize endogenous hypoxia gradients to drive morphogenetic events during normal development. Here we show that the tolerance to hypoxic conditions changes between different developmental stages of the sea urchin embryo, due to the structure of the gene regulatory networks (GRNs). We demonstrate that during normal development, bone morphogenetic protein (BMP) pathway restricts the activity of the vascular endothelial growth factor (VEGF) pathway to two lateral domains and by that controls proper skeletal patterning. Hypoxia applied during early development strongly perturbs the activity of Nodal and BMP pathways that affect VEGF pathway, dorsal-ventral (DV) and skeletogenic patterning. These pathways are largely unaffected by hypoxia applied after DV axis formation. We propose that the structure of the DV GRN, that includes feedback and feedforward loops, increases its resilience to changes of the initial oxygen gradients and helps the embryos tolerate transient hypoxia.

Key words: Hypoxia, Gene regulatory networks, Sea urchin, VEGF, BMP, Nodal, HIF1a, Deoxygenation, Evolution and development, Echinoderms, Skeletogenesis, Vascularization

Global warming leads to the reduction in dissolved molecular oxygen (O_2) and increased respiration of marine organisms; together with anthropogenic disruptions this leads to deoxygenation, oxygen loss in the ocean (Altieri et al., 2017; Breitburg et al., 2018; Hughes et al., 2020; Schmidtko et al., 2017). Studies from the last decade indicate that deoxygenation is more lethal to marine life than the direct effect of the rising temperatures or ocean acidification (Altieri et al., 2017; Breitburg et al., 2018; Hughes et al., 2020; Schmidtko et al., 2017; Vaquer-Sunyer and Duarte, 2008). Moreover, the diurnal changes in oxygen levels due to algae and phytoplankton photosynthesis, expose animals to dramatic daily changes in oxygen levels that require fast adaptation (Hughes et al., 2020). These current analyses are further supported by the geological record: a recent study shows that the marine mass extinction at the end of the Permian period can be explained by the temperature-dependent hypoxia that was lethal to marine organisms in the temperate regions (Penn et al., 2018).

During the evolution of metazoans, animals were exposed to variations in oxygen levels and molecular mechanisms evolved to enable organisms to cope with hypoxic conditions (Semenza, 2012). However, it is still unclear whether these mechanisms are sufficient to protect organisms from acute hypoxic conditions (Altieri et al., 2017; Breitburg et al., 2018; Hughes et al., 2020). Particularly, the early stages of embryogenesis could be more sensitive to deoxygenation (Vaquer-Sunyer and Duarte, 2008), as endogenous hypoxia regulates morphogenesis during normal development of vertebrates and other marine organisms (Chang et al., 2017; Coffman and Su, 2019; Dunwoodie, 2009; Lendahl et al., 2009). Understanding the molecular mechanisms that mediate the response to both physiological and environmental hypoxia during the development of marine animals is a key to understand the expected effect of ocean deoxygenation on marine biodiversity.

The sea urchin embryo provides an attractive system to study the molecular pathways that respond to variation in oxygen levels during embryogenesis. Sea urchins are major grazers in shallow seas and coastal waters across the oceans (Pearse, 2006) and adult sea urchins were shown to be moderately sensitive to hypoxic conditions (Hughes et al., 2020; Low and Micheli, 2018; Suh et al., 2014; Vaquer-Sunyer and Duarte, 2008). The role of the sea urchins in marine ecology and the experimental advantages of their embryos make them a prominent model system for ecological, evolutionary and developmental studies (Pearse, 2006; Peter and Davidson, 2011; Sethi et al., 2012). Particularly, the models of the gene regulatory networks that drive sea urchin early development are the stat of the art in the field (Morgulis et al., 2019; Oliveri et al., 2008; Peter and Davidson, 2011).

Sea urchin embryos use oxygen and redox gradients to form their dorsal-ventral (DV) axis through the modulation of several signaling pathways (Fig. 1, (Chang et al., 2017; Coffman et al., 2014; Suh et al., 2014)). In the eggs of the sea urchins, the mitochondria are concentrated at the future ventral side (Coffman et al., 2004; Coffman et al., 2014), which leads to the formation of redox and oxygen gradients in the early embryos (Fig. 1A, (Agca et al., 2009; Coffman et al., 2004)). The redox gradient activates the expression of the Nodal ligand in the ventral ectoderm (Agca et al., 2009; Coffman et al., 2004;

Coffman et al., 2014). Nodal reception drives the expression of the Nodal ligand and its antagonist Lefty and the positive and negative feedback interactions between these two proteins define the boundaries of the ventral ectoderm (Fig. 1B, (Duboc et al., 2008; Duboc et al., 2004)). Nodal activity drives the expression of the Bone Morphogenetic Protein (BMP), BMP2/4, and its antagonist Chordin, forming an incoherent feedforward loop (Fig. 1C, (Agca et al., 2009; Coffman et al., 2004; Coffman et al., 2014)). Chordin prevents the binding of BMP2/4 to its receptor at the ventral side so BMP is received only at the dorsal side where it activates gene expression through the phosphorylation of the transcription factor SMAD1/5/8 (Ben-Tabou de-Leon et al., 2013; Duboc et al., 2004; Lapraz et al., 2009) (Fig. 1C, D). Another early regulator of dorsal gene expression is the transcription factor, hypoxia-inducible factor 1α (HIF1α) that is stabilized in the dorsal side of the sea urchin blastula, apparently downstream of the oxygen gradient (Fig. 1A, B, (Ben-Tabou de-Leon et al., 2013; Chang et al., 2017; Coffman et al., 2009)). Thus, sea urchin embryos use the Nodal and BMP pathways and HIF1α to generate their DV axis downstream of redox and oxygen gradients inherited from the sea urchin egg.

Growth in hypoxic conditions leads to radialization of sea urchin embryos with prominent effects on the larval skeleton (Agca et al., 2009; Coffman et al., 2004). The skeleton of the sea urchin larvae is made of two skeletal calcite rods, the spicules, that are formed within a tubular syncytial chord produced by the skeletogenic cells (Morgulis et al., 2019; Oliveri et al., 2008). When the embryos are grown in hypoxic conditions the formation of the DV axis and the skeleton are disrupted, the spicules do not elongate properly and the embryonic morphology is significantly deformed (Agca et al., 2009; Coffman et al., 2004). Sea urchin skeletogenesis depends on the Vascular Endothelial Growth Factor (VEGF) pathway, an essential regulator of vertebrates' vascularization and of tubulogenesis in other phyla (Potente et al., 2011; Tettamanti et al., 2003; Tiozzo et al., 2008; Yoshida et al., 2010). The VEGF Receptor (VEGFR) is expressed in the sea urchin skeletogenic cells together with five transcription factors whose homologs are essential for vertebrates' vascularization (Adomako-Ankomah and Ettensohn, 2013; Duloquin et al., 2007; Morgulis et al., 2019; Sun and Ettensohn, 2014). This and other similarities between the sea urchin skeletogenic gene regulatory network (GRN) and the vertebrates' vascularization GRN suggest that these GRNs evolved from a common ancestral tubulogenesis GRN (Morgulis et al., 2019). The VEGF ligand is secreted from two lateral ectodermal domains located between the dorsal and the ventral ectoderm (Fig. 1D, (Adomako-Ankomah and Ettensohn, 2013; Duloquin et al., 2007; Morgulis et al., 2019)). VEGF expression is repressed in the ventral ectoderm by the transcription factor Not1 that is activated by Nodal signaling (Fig. 1D, (Li et al., 2012)). Yet, the regulatory links between BMP, HIF1α and VEGF signaling and how VEGF and BMP pathways are affected by hypoxia are not known.

Overall, sea urchin DV axis formation and skeletogenesis are strongly affected by hypoxic conditions and are regulated by signaling pathways that some of them mediate hypoxia-induced vascularization

during vertebrates' development, namely, BMP, VEGF and HIF1. The common use of these factors could indicate that they are a part of a conserved developmental GRN that utilizes hypoxia to control morphogenesis (Cordeiro and Tanaka, 2020), and potentially, make embryos more sensitive to deoxygenation. To understand the effect of exogenous hypoxia on sea urchin development, here we study the regulatory links between the sea urchin DV and skeletogenic GRNs during normal development and under hypoxia applied at different developmental stages. We reveal that these two GRNs are strongly connected through the interactions between the BMP and VEGF pathways and that the DV GRN is hypersensitive to hypoxia during early development but becomes relatively tolerant to low oxygen levels with developmental progression.

Results

Sea urchin BMP2/4 controls skeletal patterning and VEGF expression

We first wanted to elucidate the links between BMP and VEGF signaling and the effect of BMP signaling on skeletogenic gene expression during normal sea urchin development. To that end, we knocked-down (KD) BMP2/4 expression by the injection of translation morpholino oligonucleotides (MO) into the eggs of the Mediterranean sea urchin species, *Paracentrotus lividus* (*P. lividus*, Fig. 2, see methods for details). Embryos injected with BMP2/4 MO show two major skeletogenic phenotypes: the formation of ectopic spicules in addition to the normal two spicules (ES, Fig. 2B) and ectopic skeletal branching, where the basic structure of two spicules is still observed (EB, Fig. 2C). These observations are in agreement with previous studies of BMP perturbations (Duboc et al., 2004; Lapraz et al., 2009). The spatial expression of the *VEGF* gene expands to one side of the ectoderm in BMP morphants (detected by whole mount *in-situ* hybridization [WMISH], Fig. 2D). Since BMP signaling induces dorsal specification (Duboc et al., 2004; Lapraz et al., 2009), the expansion is most likely to the dorsal ectoderm, implying that BMP activity represses *VEGF* expression in the dorsal ectoderm.

The expansion of *VEGF* expression might explain the observed ectopic skeletal branching but not the formation of ectopic spicules detected in BMP morphants (Fig. 2B). This is since *VEGF* overexpression in sea urchin embryos induces skeletal branching but does not affect the overall pattering of the skeleton nor leads to the growth of ectopic spicules (Duloquin et al., 2007; Morgulis et al., 2019). The difference between BMP skeletal phenotypes and the weaker phenotypes of *VEGF* overexpression might be since BMP signaling regulates skeletogenic gene expression directly, through the phosphorylation of SMAD1/5/8, in addition to its effect on *VEGF* expression. Indeed, at late gastrula stage, phosphorylated SMAD1/5/8 (pSMAD1/5/8) is detected in the dorsal skeletogenic cells (Lapraz et al., 2009; Lapraz et al., 2006; Luo and Su, 2012) (Fig. 1D), where it a activates the expression of *tbx2/3* and *gatac (Duboc et al., 2010)*.

To better understand the regulatory links between the ectoderm and the mesodermal GRNs, we studied the effect of BMP2/4 KD on the spatial expression of *VEGFR* and its target gene, the Spicule-Matrix

protein 30 (SM30) (Duloquin et al., 2007; Morgulis et al., 2019). In control embryos, the expression of *VEGFR* is localized to the two skeletogenic cell clusters where the spicules first form (Fig. 2E) and the expression of *SM30* is noticeably enhanced in these clusters (Fig. 2F). BMP2/4 KD leads to two distinct expansion patterns of the expression of *VEGFR* and *SM30* (Fig. 2E, F). Some embryos show a continuous expansion of *SM30* and *VEGFR* expression throughout the dorsal skeletogenic cells which could drive the ectopic branching phenotype (EB in Fig. 2E, F). However, in some embryos *VEGFR* and *SM30* are expressed in three or four distinct cell clusters, which could be the cell clusters where ectopic spicules form in BMP2/4 KD (ES in Fig. 2E, F). The expression of *SM30* in ectopic skeletogenic cells clusters is different from its expression under *VEGF* overexpression, where the *SM30* signal increases, but the spatial expression pattern is unchanged (Duloquin et al., 2007). The level of *VEGFR* mRNA is increased in BMP2/4 MO at two days post fertilization (dpf), while the level of VEGF mRNA is largely unchanged (QPCR, Fig. 2G). These observations support a VEGF-independent regulation of the skeletogenic gene expression by BMP signaling. Together, our results show that BMP2/4 signaling controls sea urchin skeletal patterning, through the repression of *VEGF* expression in the dorsal ectoderm, and the repression of *VEGFR* and *SM30* in the dorsal skeletogenic cells.

HIF1α does not regulate skeletal patterning and VEGF expression

HIF1 is one of the most potent activators of VEGF expression during hypoxia induced vascularization in vertebrates and here we wanted to study its effect on sea urchin *VEGF* expression (Carmeliet, 2005; Pagès and Pouysségur, 2005). In the sea urchin species, *Strongylocentrotus purpuratus* (*S. purpuratus*), HIF1α KD reduced the early expression of the dorsal transcription factors, Tbx2/3 and Dlx, reduced the extension of the dorsal apex and mildly reduced the elongation of the dorsal skeletal rods (Ben-Tabou de-Leon et al., 2013; Chang et al., 2017). To study the effect of HIF1α perturbation on *VEGF* expression we injected HIF1α translation MO into the eggs of the sea urchin, *P. lividus* (Fig. 3). HIF1α KD did not result with distinct skeletogenic phenotypes, in agreement with its weak effect on *S. purpuratus* skeletogenesis (Chang et al., 2017) (Fig. 3A). The effect of HIF1α KD on *VEGF* expression was tested at two developmental time points: 15 hours post-fertilization (hpf) which is equivalent to the developmental time where HIF1α activates its dorsal target genes in *S. purpuratus*, and 19hpf, when the effect of HIF1α perturbation starts to decrease in *S. purpuratus* (Ben-Tabou de-Leon et al., 2013). HIF1α KD does not affect *VEGF* spatial expression pattern in these two time points (Fig. 2B). Additionally, HIF1α KD does not affect *VEGF*, *VEGFR* and *BMP2/4* expression level at both times while it decreases the expression level of its known target genes; *Pl-tbx2/3* and *Pl-dlx* (Fig. 2C). Thus, our results indicate that the role of HIF1α is restricted to dorsal ectoderm regulation, and does not interfere with skeletal patterning and VEGF regulation in the sea urchin embryo.

Rationale of acute early and late hypoxia treatments

We sought to study the effect of transient acute hypoxia on sea urchin skeletogenesis and gene expression under hypoxic conditions that are relevant to oxygen environmental levels and temporal changes. The larvae of the sea urchin are planktonic and are carried in the currents and can feel rapid variation of the oxygen level. Diurnal variations in oxygen levels typically occur within 4-12 hours and the measured changes are of ~50% and can be higher, depending on the activity of phytoplankton and water column mixing (Hughes et al., 2020). The sensitivity to hypoxia changes significantly between different species and for adult sea urchin the reported sub-lethal threshold for hypoxia is 1.22 mg/L O_2 (Sub-lethal threshold means that the animals survive this stress but their growth, reproduction and physiology are damaged (Vaquer-Sunyer and Duarte, 2008)). Water-quality surveys on sites where a massive mortality event occurred, detected levels of 0.5mg/L O_2 and below in the sea bed in depth of 10 meters and under (Altieri et al., 2017). We therefore studied the effect of growth in 0.4-0.5 mg/L O_2, which is severe hypoxic conditions, in 18°C, that is the typical temperature for the upper water column in the Mediterranean sea (Mavropoulou A.M, 2020).

We specifically wanted to distinguish between the effect of hypoxia applied during the formation of the DV axis and hypoxia applied after the DV axis is established (Duboc et al., 2004; Lapraz et al., 2009; Nam et al., 2007; Range et al., 2007). Starting at the early blastula, the expression of Nodal, is maintained by an auto-regulation, where Nodal signaling activates the expression of the *nodal* gene (Duboc et al., 2004; Lapraz et al., 2009; Nam et al., 2007; Range et al., 2007). This could indicate that this later phase of development is less sensitive to exogenous hypoxia (Fig. 1B). Early blastula occurs in *P. lividus* embryos under normal conditions at about 10hpf (Duboc et al., 2004; Lapraz et al., 2009), but when the embryos are grown in hypoxic conditions their development is slower and they reach this stage at 16hpf. We therefore studied the effect of growth in hypoxic conditions (0.4-0.5 mg/L O_2) for 16 hours, from fertilization and on (early hypoxia, Figs. 3-4), and from early blastula stage and on (late hypoxia, Fig. 5). We observed significant differences in the skeletogenic phenotypes and in gene expression between these two treatments (see methods for the exact protocol).

Early hypoxia strongly affects skeletal patterning and regulatory gene expression

Embryos grown for 16hpf in hypoxic conditions applied immediately from fertilization and on (early hypoxia), are viable and develop into a normally looking blastula, but show severe DV axis disruption and skeletogenic defects from the gastrula stage and on (Fig. 4A-G). This is in agreement with previous works on *S. purpuratus* and indicates that the effect of hypoxic conditions is not species specific (Agca et al., 2009; Chang et al., 2017; Coffman et al., 2009; Coffman et al., 2004; Coffman et al., 2014). At gastrula stage, most of the embryos grown in early hypoxia show irregular skeleton with several ectopic spicules (61%, Fig. 4B, C, G). At pluteus stage, the embryos show partial recovery and display two major skeletogenic phenotypes: A strong phenotype where the skeleton is radialized, the DV axis is disrupted and multiple ectopic spicules are observed (24%, Fig. 4F, G) and a weaker phenotype where the DV axis seem normal but the skeleton shows ectopic spicule branching (41%, Fig. 4E, G). The rest

of the embryos developed normally. The skeletogenic phenotypes indicate that hypoxic conditions can strongly affect skeletal patterning probably through changes in skeletogenic gene expression.

Next, we investigated the effect of hypoxia on the expression of the DV patterning genes, *nodal*, *BMP2/4* and *chordin*, at blastula and gastrula stages in *P. lividus*. Growth in hypoxic conditions significantly expands *nodal* spatial expression throughout the ectoderm at blastula stage, compared to the ventral localized expression of this gene in normal development (Fig. 4H), in agreement with previous studies in *S. purpuratus* (Coffman et al., 2014). The spatial expression of *BMP2/4* and *chordin* show similar expansion at this time, as expected from downstream target genes of Nodal signaling (Fig. 4I, J). At early gastrula stage, the expression of *nodal* and *BMP2/4* is expanded in embryos grown in hypoxic conditions compared to the expression of these genes in embryos grown in normoxic conditions (Fig. 4K, L). However, the expansion at gastrula stage is not throughout the ectoderm like in the blastula stage, but seems more localized to about a half of the ectoderm, in agreement with the partial phenotypic recovery at the pluteus stage.

These results suggest that hypoxia leads to the expansion of the ventral ectoderm and probably to the decrease in the dorsal ectoderm domain, which may affect the expression of key skeletogenic regulators, such as *VEGF* and *VEGFR*. Indeed, growth in hypoxic conditions shifts and expands the spatial expression of *VEGF* to one side of the ectoderm (Fig. 4M). In addition, the expression of *VEGFR* expands beyond the two lateral skeletogenic cell clusters in which it is normally localized (Fig. 4N). Furthermore, the *VEGFR* expressing cells demonstrate the perturbed migration of the skeletogenic cells in hypoxic embryos. This phenotype could be due to the expanded expression of the VEGF ligand that directs the migration of the skeletogenic cells in normal embryos. In sum, growth in hypoxic conditions perturbs the spatial organization of the skeletogenic cells and expands the ectodermal expression of *Nodal*, *BMP2/4*, *chordin* and *VEGF* and the skeletogenic expression of *VEGFR.*

Early hypoxia is mediated through the reduction in BMP activity

The expansion of the ventral side in hypoxic conditions suggests that BMP activity at the dorsal side might be reduced, and the reduction of the repressing BMP activity could explain *VEGF* expansion to the dorsal side. To test this hypothesis and monitor BMP activity in normal vs. hypoxic condition, we performed immunostaining against pSMAD1/5/8. We studied pSMAD1/5/8 signal at two different developmental stages; mesenchyme blastula, when BMP activity is localized at the dorsal ectoderm (Fig. 5A), and at late gastrula, when BMP activity is localized at the dorsal skeletogenic cells (Fig. 5C). Hypoxic conditions completely abolish pSMAD1/5/8 signal from the nuclei of the dorsal ectodermal cells at mesenchyme blastula stage (Fig. 5B). At late gastrula stage, hypoxic conditions eliminate the pSMAD1/5/8 signal from the dorsal skeletogenic cells (Fig. 5D), or strongly reduce it (Fig. 5E). These results indicate, that despite *BMP2/4* expansion in hypoxic embryos, its activity is reduced during hypoxia. The reduced activity can be explained by the expansion of BMP antagonist, Chordin, during

hypoxic conditions (Fig. 5C). Together, these results show that BMP activity in the dorsal ectoderm and in the dorsal skeletogenic cells is reduced in hypoxic conditions. Apparently, the reduction of BMP activity removes the repression of *VEGF* and *VEGFR* at the dorsal embryonic domains, leads to their expansion and disrupts skeletal patterning.

Late hypoxia mildly affects skeletogenesis and doesn't affect upstream patterning genes

Our studies show that early hypoxia strongly affects the spatial activity of the main regulators of DV axis formation, Nodal and BMP2/4, and the perturbation of these factors mediate the hypoxia effect on skeletal patterning and on *VEGF*, *VEGFR* and SM30 expression. Next, we wanted to test whether hypoxia affects skeletogenesis after the DV axis is formed and to investigate the effect of late hypoxic conditions on gene expression. Thus, we studied the skeletogenic phenotypes of hypoxia applied between 10hpf and 26hpf, which is after the DV axis is established as explained above. Embryos grown in late hypoxia showed a delayed development and at 26hpf were equivalent to early gastrula stage in normoxic embryos (Fig. 6A, B). At late gastrula and pluteus stages, almost all the embryos grown in late hypoxia show normal skeletal patterning with the two spicules correctly positioned at the two lateral sides (Fig. 6C-G). More than half of the embryos grown in late hypoxia developed ectopic skeletal branching in these two stages, and at pluteus stage, about 2% of the embryos show radialized skeleton with ectopic spicules. Overall, late hypoxia induces skeletal defects, such as ectopic branching, but it hardly affects skeletal patterning.

We next studied the effect of late hypoxic conditions on the expression of the key regulatory genes investigated above. Late hypoxia treatment does not affect the spatial expression of *nodal* (Fig. 6H), in agreement with the normal formation of the DV axis and normal skeletal patterning in this condition. Furthermore, late hypoxia does not affect the spatial expression pattern of *BMP2/4*, *VEGF* and *VEGFR* genes, so these genes are probably not the mediators of the observed skeletal defects (Fig. 6I-K). Thus, after the DV axis forms, the expression of the upstream patterning and skeletogenesis regulators, *nodal*, *BMP2/4*, *VEGF* and *VEGFR* is not affected by hypoxic conditions and the skeletal patterning seem to be normal.

Discussion

Animals evolved a common molecular tool kit to protect them from variations in oxygen level (Cordeiro and Tanaka, 2020; Dunwoodie, 2009), yet, the geological record tells us that these molecular mechanisms might not be sufficient to sustain life in warmer and more hypoxic oceans (Penn et al., 2018). Particularly, the use of hypoxia to control different developmental processes in various phyla, might make the embryos more sensitive to hypoxic conditions (Compernolle et al., 2003; Cordeiro and Tanaka, 2020; Dunwoodie, 2009; Semenza, 2012). Here we studied the regulatory linkages and response to transient acute hypoxia of the GRNs that control DV patterning and skeletogenesis in the sea urchin embryo (Fig. 7A, B). We discovered that the structure of these GRNs makes them very

sensitive to hypoxic conditions applied at early development, but quite tolerant to these conditions if they occur later in development. The resemblance between the hypoxia-induced GRN that patterns the skeleton of the sea urchin embryo and the vertebrates' vascularization GRN, might explain the sensitivity of marine vertebrates' embryos to growth in hypoxic conditions (Barrionuevo et al., 2010; Crossley and Altimiras, 2005; Del Rio et al., 2019; Hassell et al., 2008; Metikala et al., 2016; Shang and Wu, 2004).

Our and previous studies show that in the sea urchin embryo, ectodermal VEGF and BMP signaling provide the activating and inhibiting cues that guide normal skeletal patterning: VEGF activates the expression of skeletogenic genes and drives skeleton formation (Adomako-Ankomah and Ettensohn, 2013; Duloquin et al., 2007; Morgulis et al., 2019; Sun and Ettensohn, 2014), while BMP2/4 restricts VEGF, VEGFR and skeletogenic gene expression into two localized domains of active skeletal growth (Fig. 2A-F, Fig. 7A). Hence, the opposing interactions between VEGF and BMP2/4 are necessary for the correct spatial expression of skeletogenic genes and for correct skeletal patterning in normal development.

Early hypoxia in sea urchin embryos strongly distorts DV and skeletogenic patterning due to its strong effect on the key DV patterning gene, Nodal that controls BMP activity (Fig. 7A,B); however, late hypoxia doesn't affect Nodal expression, apparently since it is maintained by auto-regulation at this time (Nam et al., 2007; Range et al., 2007). Early hypoxia leads to the expansion of *nodal* to the dorsal side, which leads to the expansion of its targets, *BMP2/4* and *chordin* (Fig. 7B). The expansion of Chordin into the dorsal side leads to the reduction of BMP activity in this side, which removes the dorsal repression of *VEGF* and *VEGFR* expression which drives the growth of ectopic spicules in the dorsal side (Fig. 7B). At the early blastula stage, Nodal expression is maintained by the Nodal pathway through the transcription factor SMAD2/3 (Nam et al., 2007; Range et al., 2007), and *nodal* spatial expression is restricted by its antagonist, Lefty, that is also activated by the Nodal pathway (Fig. 1B, (Duboc et al., 2008)). These positive and negative feedback interactions could underlie the relative restriction of *nodal* expression at the gastrula stage compared to its broad expression at the blastula stage (Fig. 4H, K) and the partial recovery of skeletal patterning in the pluteus stage compared to the gastrula stage (Fig. 4G). The structure of the DV GRN also explains the robustness of DV and skeletogenic patterning genes to late hypoxia. Once the spatial domain of Nodal activity is established and stabilized by the Nodal-Lefty feedback loops, it defines the domain of BMP activity through the Nodal-BMP2/4-Chordin incoherent feedforward loop, which restricts VEGF activity, and normal patterning is observed (Fig. 7A). Overall, the structure of the DV GRN enables it to partially recover early hypoxia at later developmental stages and makes the GRN resilient to late hypoxia.

Our findings illuminate the similarities between the DV patterning and skeletogenic GRNs and the hypoxia-induced regulation of vertebrate's vascularization. The similarities include the regulatory interactions between VEGF and BMP pathways and the participation of HIF1 and Nodal in the response

to hypoxic conditions (compare Fig. 7A, B with 7C). The regulatory interactions between BMP and VEGF control vertebrates' vascularization, however, they are rather complex, as BMP activates VEGF and induces vascularization in some tissues, while it represses VEGF in other tissues (Bai et al., 2013; Dyer et al., 2014; Garcia de Vinuesa et al., 2016; He and Chen, 2005; Wiley et al., 2011). Evidently, the complexity of the BMP and VEGF pathways in vertebrates is much higher than in echinoderms due to the whole genome duplication (Kassahn et al., 2009; Singh et al., 2015) that resulted with higher number of pathway components which could support the evolution of more intricate interactions. The Nodal pathway does not participate in hypoxia induced vascularization during normal development in vertebrates, however, in various cancer cells, hypoxia drives Nodal expression, which then promotes *VEGF* expression and angiogenesis (Fig. 7C, (Hueng et al., 2011; Quail et al., 2011; Quail et al., 2012)). HIF1α, a major activator of VEGF in vertebrates' hypoxia-induced vascularization ((Dunwoodie, 2009; Pagès and Pouysségur, 2005), Fig. 7C) participates in DV axis formation in the sea urchin embryo, but does not regulate VEGF signaling (Fig. 7A). Overall, complex regulatory interactions between Nodal, BMP, HIF1 and VEGF pathways and their modulation by hypoxic conditions are observed both during DV and skeletal patterning in the sea urchin embryo and in vertebrates' vascularization (Fig. 7). These common interactions together with the similarity between the skeletogenic GRN and the vascularization GRN (Morgulis et al., 2019; Oliveri et al., 2008) could be explained by the divergence of these two patterning programs from a common ancestral GRN.

Within the observed similarities between the patterning GRNs of sea urchin skeletogenesis and vertebrates' vascularization, there is a distinct difference: the sea urchin GRN is only temporarily sensitive to hypoxia while hypoxia drives vascularization throughout vertebrates development, in adult ischemic tissues and in cancer (Carmeliet, 2005; Dunwoodie, 2009; Dyer et al., 2014; Garcia de Vinuesa et al., 2016; Hueng et al., 2011; Kim et al., 2014; Pagès and Pouysségur, 2005; Quail et al., 2012). This could indicate that the sensitivity of vertebrates' embryos to hypoxic conditions lingers throughout the development of their vascular system, and possibly beyond this time. Relatedly, vertebrate embryos show high sensitivity to growth in hypoxic conditions (Barrionuevo et al., 2010; Crossley and Altimiras, 2005; Del Rio et al., 2019; Hassell et al., 2008; Metikala et al., 2016; Shang and Wu, 2004), with specific defects in the cardiovascular and vascular systems (Compernolle et al., 2003; Crossley and Altimiras, 2005; Metikala et al., 2016). Thus, utilizing the same molecular mechanisms that protect organisms from low oxygen level for morphogenesis, possibly makes the embryos of these organisms more vulnerable to hypoxic conditions.

Establishing the biological hypoxia thresholds that distinguish waterbodies that endanger their habitat from those that support them is a major challenge in marine conservation (Vaquer-Sunyer and Duarte, 2008). Since it is hard to monitor embryos, the main biological indicator is the health of adult organisms; yet embryogenesis might be the most sensitive stage on an organism's life. The comprehensive models of the sea urchin developmental GRNs help us decipher how the resilience of the sea urchin embryo to

transient hypoxic conditions increases with developmental time. Further genetic studies guided by environmental changes might elucidate the sensitivity and resilience of the molecular response to hypoxia in marine embryos and enable a better design of conservation plans for marine life.

Materials and Methods

Animals and embryo cultures

Adult *P. lividus* sea urchins were purchased from the Institute of Oceanographic and Limnological Research (IOLR) in Eilat, Israel. Eggs and sperm were obtained by injection 0.5M KCl solution to adult sea urchins. Embryos were cultured in artificial seawater (ASW) at 18°C.

Microinjection, RNA extraction and Reverse-transcription

The design and preparation of novel morpholino (MO) was done in genetools (http://www.gene-tools.com). Translation of *HIF1α* was blocked by the microinjection of 400-700µM *HIF1α*-MO into sea urchin eggs. *HIF1α*-MO sequence: 5`-GGTCGCCATAATCAGTCTCTGTTTC-3`. Translation of *BMP2/4* was blocked by the microinjection of 400-600µM. *BMP2/4*-MO sequence: 5`-GACCCAGTTTGAGGTGGTAACCAT-3`, this MO has been characterized in previous studies (Duboc et al., 2004). The control MO is Random commercial MO which does not have any effect on embryo development, along with 1µg/ml rhodamine dextran (D3329 Molecular probes, OR, USA) and 0.12M KCl. Total RNA was extracted from injected sea urchin embryos (≥120 injected embryos) using RNeasy Micro Kit (50) from QIAGEN (#74004) according to the kit protocol using DNase treatment from RNease-Free DNase Set- Qiagen (50) (#79254). Elution was done in 16.5µl nuclease-free ultra-pure water. Extracted RNAs were then reverse transcribed into cDNA by using SuperScript™ II Reverse Transcriptase (Thermo Fisher scientific 18064022) (10 min 25°C, 2hr in 25°C, 85°C for 5 min).

Quantitative-PCR (qPCR) analysis

qPCR was performed using the CFX384 Touch™ Real-Time PCR Detection System #1855485. Reactions were carried out in 10µl volume including: 5µl SYBR BioRad IQ SYBR Green Supermix (#1725125), 2.5µl of 1.2µM forward and reverse gene specific primers and 2.5µl of cDNA (qPCR primers used in this study are listed in Table S1). Each cDNA sample was run in triplicate, for every candidate gene, ubiquitin was used as internal control. The reactions thermal profile was: 95°C for 3 minutes followed by 40 amplification cycles of 95°C for 10 seconds and 55°C for 30 sec. Dissociation analysis was performed at the end of each reaction to confirm the amplification specificity. Primer sets for all tested genes were designed using Primer3Plus (http://www.bioinformatics.nl/ cgi-bin/primer3plus/primer3plus.cgi/). Results are presented as the means and standard error of at least two biological replicates. The comparison to an internal standard (ubiquitin) was done in order to determine the expression level of the gene, and the change in the expression levels were measured in comparison to the expression level of the gene in control MO.

Hypoxia treatment

ASW were treated with 99.5% Nitrogen (N_2) and 0.5% Oxygen (O_2) to decrease the oxygen solubility in ASW till the dissolved O_2 level was 0.4-0.5 mg/L, creating hypoxic ASW. Embryos were transferred into petri-dish that contains the hypoxic ASW, then the dishes were incubated in a hypoxia chamber at 18°C. The hypoxia chamber is a sealed box that receives a constant flow of 99.5% N_2 and 0.5% O_2. To distinguish between the direct effect that hypoxic conditions might have on skeletogenesis and its effect on DV patterning, we studied the skeletogenic phenotypes of hypoxia applied immediately after fertilization (early hypoxic condition) and the effect of hypoxia applied after the DV axis was established (late hypoxic condition). In early hypoxia treatment, the eggs were fertilized, their fertilization envelope was immediately removed and the zygotes were incubated in the hypoxia chamber for 16 hours. In late hypoxia treatment, the eggs were fertilized and the embryos were cultured under normoxic conditions for 10 hours until the blastula stage. Then, the embryos were transferred into the hypoxia chamber and incubated in hypoxic conditions for 16 hours. After 16 hours in hypoxic conditions the embryos were removed from the hypoxia chamber and cultured in normoxic conditions until the pluteus stage.

Probe design and WMISH procedure

WMISH probe preparation and WMISH procedure were performed as described in(Morgulis et al., 2019). Primer list is provided in table S2.

Removal of fertilization envelope

To perform WMISH on sea urchin embryos at early blastula stage, the fertilization envelope were removed; Fertilized eggs were incubated in presence of Paraminobenzoic acid (PABA, A6928, Sigma) and Amino triazole (ATA, A8056 Sigma) (2mM each at final concentration) to soften the fertilization envelope (FE). After microscopy visualization of FE, FE were removed by flow the zygotes through a 75µm mesh four times. Next, the embryos were washed three times with ASW and grown till the indicated collection time points.

Immunostaining

Immunostaining of pSMAD1/5/8 antibody was done similarly to (Lapraz et al., 2009) with minor modifications. Embryos were fixed in 4% paraformaldehyde, 33mM Maleic acid buffer pH7, 166mM NaCl, for 10 minutes at room temperature, then embryos exposed to Methanol for 1 minute. Embryos were washed four times with PBST, then incubation for 1 hour in blocking solution (PBST and 4% sheep serum), followed by incubation with primary Antibody against pSMAD1/5/8 (the antibody was purchased from Cell Signaling Technology; no. 9511) at 1:200 dilution in blocking solution, overnight at 4˚C. Embryos were then washed four time in PBST, then the secondary Antibody was added to the embryos (Peroxidase-conjugated AffiniPure Goat Anti-Rabbit IgG; no. 111-035-003) diluted 1:200 in

blocking solution and incubated for 1 hour in room temperature, followed by four washes with PBST. Store solution (PBST in 50% glycerol) at 4˚C.

Imaging

All images presented in this study were generated on a Zeiss Axio Imager M2.

Acknowledgments

We thank Imad Shams for generously providing the hypoxic chamber and gas controller; Eli shemesh for providing the oxygen sensor; Shlomo Ben-Tabou de-Leon for technical assistance with the hypoxic system build-up; David Ben-Ezra for his help with sea urchin handling; Miri Morgulis for helpful comments and suggestions. This work was supported by the Israel Science Foundation Grant 41/14 (to Smadar Ben-Tabou de-Leon).

References

Adomako-Ankomah, A., Ettensohn, C.A., 2013. Growth factor-mediated mesodermal cell guidance and skeletogenesis during sea urchin gastrulation. Development 140, 4214-4225.

Agca, C., Klein, W.H., Venuti, J.M., 2009. Reduced O2 and elevated ROS in sea urchin embryos leads to defects in ectoderm differentiation. Dev Dyn 238, 1777-1787.

Altieri, A.H., Harrison, S.B., Seemann, J., Collin, R., Diaz, R.J., Knowlton, N., 2017. Tropical dead zones and mass mortalities on coral reefs. Proc Natl Acad Sci U S A 114, 3660-3665.

Bai, Y., Wang, J., Morikawa, Y., Bonilla-Claudio, M., Klysik, E., Martin, J.F., 2013. Bmp signaling represses Vegfa to promote outflow tract cushion development. Development 140, 3395-3402.

Barrionuevo, W.R., Fernandes, M.N., Rocha, O., 2010. Aerobic and anaerobic metabolism for the zebrafish, Danio rerio, reared under normoxic and hypoxic conditions and exposed to acute hypoxia during development. Braz J Biol 70, 425-434.

Ben-Tabou de-Leon, S., Su, Y.H., Lin, K.T., Li, E., Davidson, E.H., 2013. Gene regulatory control in the sea urchin aboral ectoderm: spatial initiation, signaling inputs, and cell fate lockdown. Dev Biol 374, 245-254.

Breitburg, D., Levin, L.A., Oschlies, A., Gregoire, M., Chavez, F.P., Conley, D.J., Garcon, V., Gilbert, D., Gutierrez, D., Isensee, K., Jacinto, G.S., Limburg, K.E., Montes, I., Naqvi, S.W.A., Pitcher, G.C., Rabalais, N.N., Roman, M.R., Rose, K.A., Seibel, B.A., Telszewski, M., Yasuhara, M., Zhang, J., 2018. Declining oxygen in the global ocean and coastal waters. Science 359.

Carmeliet, P., 2005. VEGF as a key mediator of angiogenesis in cancer. Oncology 69 Suppl 3, 4-10.

Chang, W.L., Chang, Y.C., Lin, K.T., Li, H.R., Pai, C.Y., Chen, J.H., Su, Y.H., 2017. Asymmetric distribution of hypoxia-inducible factor alpha regulates dorsoventral axis in the early sea urchin embryo. Development.

Coffman, J.A., Coluccio, A., Planchart, A., Robertson, A.J., 2009. Oral-aboral axis specification in the sea urchin embryo III. Role of mitochondrial redox signaling via H2O2. Dev Biol 330, 123-130.

Coffman, J.A., Davidson, E.H., 2001. Oral-aboral axis specification in the sea urchin embryo. I. Axis entrainment by respiratory asymmetry. Dev Biol 230, 18-28.

454 Coffman, J.A., McCarthy, J.J., Dickey-Sims, C., Robertson, A.J., 2004. Oral–aboral axis
455 specification in the sea urchin embryo: II. Mitochondrial distribution and redox state
456 contribute to establishing polarity in Strongylocentrotus purpuratus. Dev Biol 273, 160-171.
457 Coffman, J.A., Su, Y.H., 2019. Redox regulation of development and regeneration. Curr Opin
458 Genet Dev 57, 9-15.
459 Coffman, J.A., Wessels, A., DeSchiffart, C., Rydlizky, K., 2014. Oral-aboral axis specification in
460 the sea urchin embryo, IV: hypoxia radializes embryos by preventing the initial spatialization
461 of nodal activity. Dev Biol 386, 302-307.
462 Compernolle, V., Brusselmans, K., Franco, D., Moorman, A., Dewerchin, M., Collen, D.,
463 Carmeliet, P., 2003. Cardia bifida, defective heart development and abnormal neural crest
464 migration in embryos lacking hypoxia-inducible factor-1alpha. Cardiovasc Res 60, 569-579.
465 Cordeiro, I.R., Tanaka, M., 2020. Environmental Oxygen is a Key Modulator of Development
466 and Evolution: From Molecules to Ecology: Oxygen-sensitive pathways pattern the
467 developing organism, linking genetic and environmental components during the evolution
468 of new traits. Bioessays, e2000025.
469 Crossley, D.A., 2nd, Altimiras, J., 2005. Cardiovascular development in embryos of the
470 American alligator Alligator mississippiensis: effects of chronic and acute hypoxia. J Exp Biol
471 208, 31-39.
472 Czihak, G., 1963. Entwicklungsphysiologische untersuchungen an echiniden. Wilhelm
473 Roux'Archiv für Entwicklungsmechanik der Organismen 154, 272-292.
474 Del Rio, A.M., Davis, B.E., Fangue, N.A., Todgham, A.E., 2019. Combined effects of warming
475 and hypoxia on early life stage Chinook salmon physiology and development. Conserv
476 Physiol 7, coy078.
477 Duboc, V., Lapraz, F., Besnardeau, L., Lepage, T., 2008. Lefty acts as an essential modulator
478 of Nodal activity during sea urchin oral-aboral axis formation. Dev Biol 320, 49-59.
479 Duboc, V., Lapraz, F., Saudemont, A., Bessodes, N., Mekpoh, F., Haillot, E., Quirin, M.,
480 Lepage, T., 2010. Nodal and BMP2/4 pattern the mesoderm and endoderm during
481 development of the sea urchin embryo. Development 137, 223-235.
482 Duboc, V., Rottinger, E., Besnardeau, L., Lepage, T., 2004. Nodal and BMP2/4 signaling
483 organizes the oral-aboral axis of the sea urchin embryo. Dev Cell 6, 397-410.
484 Duloquin, L., Lhomond, G., Gache, C., 2007. Localized VEGF signaling from ectoderm to
485 mesenchyme cells controls morphogenesis of the sea urchin embryo skeleton. Development
486 134, 2293-2302.
487 Dunwoodie, S.L., 2009. The role of hypoxia in development of the Mammalian embryo. Dev
488 Cell 17, 755-773.
489 Dyer, L.A., Pi, X., Patterson, C., 2014. The role of BMPs in endothelial cell function and
490 dysfunction. Trends Endocrinol Metab 25, 472-480.
491 Garcia de Vinuesa, A., Abdelilah-Seyfried, S., Knaus, P., Zwijsen, A., Bailly, S., 2016. BMP
492 signaling in vascular biology and dysfunction. Cytokine Growth Factor Rev 27, 65-79.
493 Hassell, K.L., Coutin, P.C., Nugegoda, D., 2008. Hypoxia impairs embryo development and
494 survival in black bream (Acanthopagrus butcheri). Marine pollution bulletin 57, 302-306.
495 He, C., Chen, X., 2005. Transcription regulation of the vegf gene by the BMP/Smad pathway
496 in the angioblast of zebrafish embryos. Biochem Biophys Res Commun 329, 324-330.
497 Hueng, D.-Y., Lin, G.-J., Huang, S.-H., Liu, L.-W., Ju, D.-T., Chen, Y.-W., Sytwu, H.-K., Chang, C.,
498 Huang, S.-M., Yeh, Y.-S., 2011. Inhibition of Nodal suppresses angiogenesis and growth of
499 human gliomas. Journal of neuro-oncology 104, 21-31.

500 Hughes, D.J., Alderdice, R., Cooney, C., Kühl, M., Pernice, M., Voolstra, C.R., Suggett, D.J.,
501 2020. Coral reef survival under accelerating ocean deoxygenation. Nature Climate Change
502 10, 296-307.
503 Kassahn, K.S., Dang, V.T., Wilkins, S.J., Perkins, A.C., Ragan, M.A., 2009. Evolution of gene
504 function and regulatory control after whole-genome duplication: comparative analyses in
505 vertebrates. Genome Res 19, 1404-1418.
506 Kim, J.-D., Lee, H.-W., Jin, S.-W., 2014. Diversity is in my veins: role of bone morphogenetic
507 protein signaling during venous morphogenesis in zebrafish illustrates the heterogeneity
508 within endothelial cells. Arterioscler Thromb Vasc Biol 34, 1838-1845.
509 Lapraz, F., Besnardeau, L., Lepage, T., 2009. Patterning of the Dorsal-Ventral Axis in
510 Echinoderms: Insights into the Evolution of the BMP-Chordin Signaling Network. PLOS
511 Biology 7, e1000248.
512 Lapraz, F., Röttinger, E., Duboc, V., Range, R., Duloquin, L., Walton, K., Wu, S.-Y., Bradham,
513 C., Loza, M.A., Hibino, T., Wilson, K., Poustka, A., McClay, D., Angerer, L., Gache, C., Lepage,
514 T., 2006. RTK and TGF-β signaling pathways genes in the sea urchin genome. Dev Biol 300,
515 132-152.
516 Lendahl, U., Lee, K.L., Yang, H., Poellinger, L., 2009. Generating specificity and diversity in
517 the transcriptional response to hypoxia. Nat Rev Genet 10, 821-832.
518 Li, E., Materna, S.C., Davidson, E.H., 2012. Direct and indirect control of oral ectoderm
519 regulatory gene expression by Nodal signaling in the sea urchin embryo. Dev Biol 369, 377-
520 385.
521 Low, N.H.N., Micheli, F., 2018. Lethal and functional thresholds of hypoxia in two key
522 benthic grazers. Marine Ecology Progress Series 594, 165-173.
523 Luo, Y.J., Su, Y.H., 2012. Opposing nodal and BMP signals regulate left-right asymmetry in
524 the sea urchin larva. PLoS Biol 10, e1001402.
525 Mavropoulou A.M, V.V., Sofianos S., 2020. Dissolved oxygen variability in the Mediterranean
526 Sea. J Mar Syst 208, 103348.
527 Metikala, S., Neuhaus, H., Hollemann, T., 2016. Suppression of vascular network formation
528 by chronic hypoxia and prolyl-hydroxylase 2 (phd2) deficiency during vertebrate
529 development. Angiogenesis 19, 119-131.
530 Morgulis, M., Gildor, T., Roopin, M., Sher, N., Malik, A., Lalzar, M., Dines, M., Ben-Tabou de-
531 Leon, S., Khalaily, L., Ben-Tabou de-Leon, S., 2019. Possible cooption of a VEGF-driven
532 tubulogenesis program for biomineralization in echinoderms. Proceedings of the National
533 Academy of Sciences 116, 12353.
534 Nam, J., Su, Y.H., Lee, P.Y., Robertson, A.J., Coffman, J.A., Davidson, E.H., 2007. Cis-
535 regulatory control of the nodal gene, initiator of the sea urchin oral ectoderm gene network.
536 Dev Biol 306, 860-869.
537 Oliveri, P., Tu, Q., Davidson, E.H., 2008. Global regulatory logic for specification of an
538 embryonic cell lineage. Proc Natl Acad Sci U S A 105, 5955-5962.
539 Pagès, G., Pouysségur, J., 2005. Transcriptional regulation of the Vascular Endothelial
540 Growth Factor gene–a concert of activating factors*. Cardiovascular Research 65, 564-573.
541 Pearse, J.S., 2006. Ecological role of purple sea urchins. Science 314, 940-941.
542 Penn, J.L., Deutsch, C., Payne, J.L., Sperling, E.A., 2018. Temperature-dependent hypoxia
543 explains biogeography and severity of end-Permian marine mass extinction. Science 362.
544 Peter, I.S., Davidson, E.H., 2011. A gene regulatory network controlling the embryonic
545 specification of endoderm. Nature 474, 635-639.

546 Potente, M., Gerhardt, H., Carmeliet, P., 2011. Basic and therapeutic aspects of
547 angiogenesis. Cell 146, 873-887.
548 Quail, D.F., Taylor, M.J., Walsh, L.A., Dieters-Castator, D., Das, P., Jewer, M., Zhang, G.,
549 Postovit, L.M., 2011. Low oxygen levels induce the expression of the embryonic morphogen
550 Nodal. Mol Biol Cell 22, 4809-4821.
551 Quail, D.F., Walsh, L.A., Zhang, G., Findlay, S.D., Moreno, J., Fung, L., Ablack, A., Lewis, J.D.,
552 Done, S.J., Hess, D.A., Postovit, L.-M., 2012. Embryonic Protein Nodal Promotes Breast
553 Cancer Vascularization. Cancer Research 72, 3851.
554 Range, R., Lapraz, F., Quirin, M., Marro, S., Besnardeau, L., Lepage, T., 2007. Cis-regulatory
555 analysis of nodal and maternal control of dorsal-ventral axis formation by Univin, a TGF-beta
556 related to Vg1. Development 134, 3649-3664.
557 Schmidtko, S., Stramma, L., Visbeck, M., 2017. Decline in global oceanic oxygen content
558 during the past five decades. Nature 542, 335-339.
559 Semenza, G.L., 2012. Hypoxia-inducible factors in physiology and medicine. Cell 148, 399-
560 408.
561 Sethi, A.J., Wikramanayake, R.M., Angerer, R.C., Range, R.C., Angerer, L.M., 2012. Sequential
562 signaling crosstalk regulates endomesoderm segregation in sea urchin embryos. Science
563 335, 590-593.
564 Shang, E.H., Wu, R.S., 2004. Aquatic hypoxia is a teratogen and affects fish embryonic
565 development. Environ Sci Technol 38, 4763-4767.
566 Singh, P.P., Arora, J., Isambert, H., 2015. Identification of Ohnolog Genes Originating from
567 Whole Genome Duplication in Early Vertebrates, Based on Synteny Comparison across
568 Multiple Genomes. PLoS Comput Biol 11, e1004394.
569 Suh, S.S., Hwang, J., Park, M., Park, S.Y., Ryu, T.K., Lee, S., Lee, T.K., 2014. Hypoxia-
570 modulated gene expression profiling in sea urchin (Strongylocentrotus nudus) immune cells.
571 Ecotoxicol Environ Saf 109, 63-69.
572 Sun, Z., Ettensohn, C.A., 2014. Signal-dependent regulation of the sea urchin skeletogenic
573 gene regulatory network. Gene Expression Patterns 16, 93-103.
574 Tettamanti, G., Grimaldi, A., Valvassori, R., Rinaldi, L., de Eguileor, M., 2003. Vascular
575 endothelial growth factor is involved in neoangiogenesis in Hirudo medicinalis (Annelida,
576 Hirudinea). Cytokine 22, 168-179.
577 Tiozzo, S., Voskoboynik, A., Brown, F.D., De Tomaso, A.W., 2008. A conserved role of the
578 VEGF pathway in angiogenesis of an ectodermally-derived vasculature. Dev Biol 315, 243-
579 255.
580 Vaquer-Sunyer, R., Duarte, C.M., 2008. Thresholds of hypoxia for marine biodiversity. Proc
581 Natl Acad Sci U S A 105, 15452-15457.
582 Wiley, D.M., Kim, J.-D., Hao, J., Hong, C.C., Bautch, V.L., Jin, S.-W., 2011. Distinct signalling
583 pathways regulate sprouting angiogenesis from the dorsal aorta and the axial vein. Nature
584 Cell Biology 13, 686-692.
585 Yoshida, M.A., Shigeno, S., Tsuneki, K., Furuya, H., 2010. Squid vascular endothelial growth
586 factor receptor: a shared molecular signature in the convergent evolution of closed
587 circulatory systems. Evol Dev 12, 25-33.
588
589
590
591
592
593

594

Figures

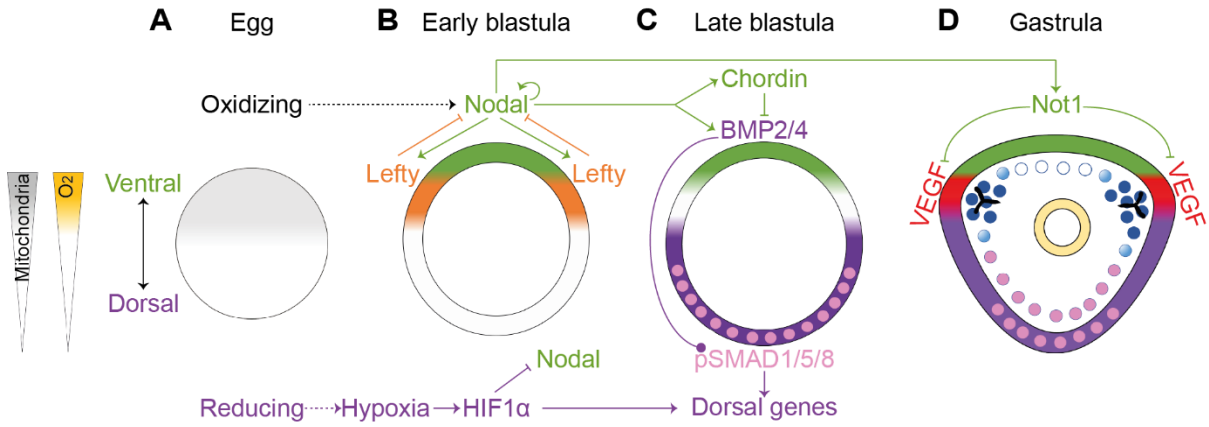

Figure 1 The regulation of DV axis formation downstream of redox and oxygen gradients in the sea urchin embryo. Diagrams showing sea urchin DV and skeletal patterning in normal conditions based on(Chang et al., 2017; Coffman et al., 2009; Coffman and Davidson, 2001; Coffman et al., 2004; Coffman et al., 2014; Czihak, 1963; Duboc et al., 2004; Lapraz et al., 2009; Li et al., 2012). **(A)** The asymmetric distribution of mitochondria in the egg induces a redox gradient. **(B)** At the early blastula stage, redox and oxygen gradients activate the ligand Nodal in the ventral ectoderm and stabilize HIF1α activity in the dorsal side. HIF1α activates dorsal genes and transiently represses nodal expression in the dorsal ectoderm. Nodal activity in the ventral ectoderm activates its own ligand expression (positive feedback) and the expression of its antagonist lefty (negative feedback), that diffuses further than Nodal and by that restricts Nodal activity to the ventral domain. **(C)** In the late blastula stage, Nodal activates the expression of BMP2/4 and Chordin in the ventral ectoderm, and that forms an incoherent feedforward loop as Chordin antagonizes BMP2/4 activity in the ventral ectoderm. BMP2/4 protein translocates to the dorsal side and induces the phosphorylation of the transcription factor SMAD1/5/8 that activates dorsal genes. **(D)** In the gastrula stage, Nodal activates the expression of Not1, that represses VEGF expression in the ventral ectoderm, and restricts VEGF expression to two lateral ectodermal domains. The ventral side and Nodal expression domain are highlighted in green. The dorsal side and the domain of BMP activity are marked in purple. Nucleus that show pSMAD1/5/8 are highlighted in pink. VEGF expression is marked in red. VEGFR is expression is marked in blue.

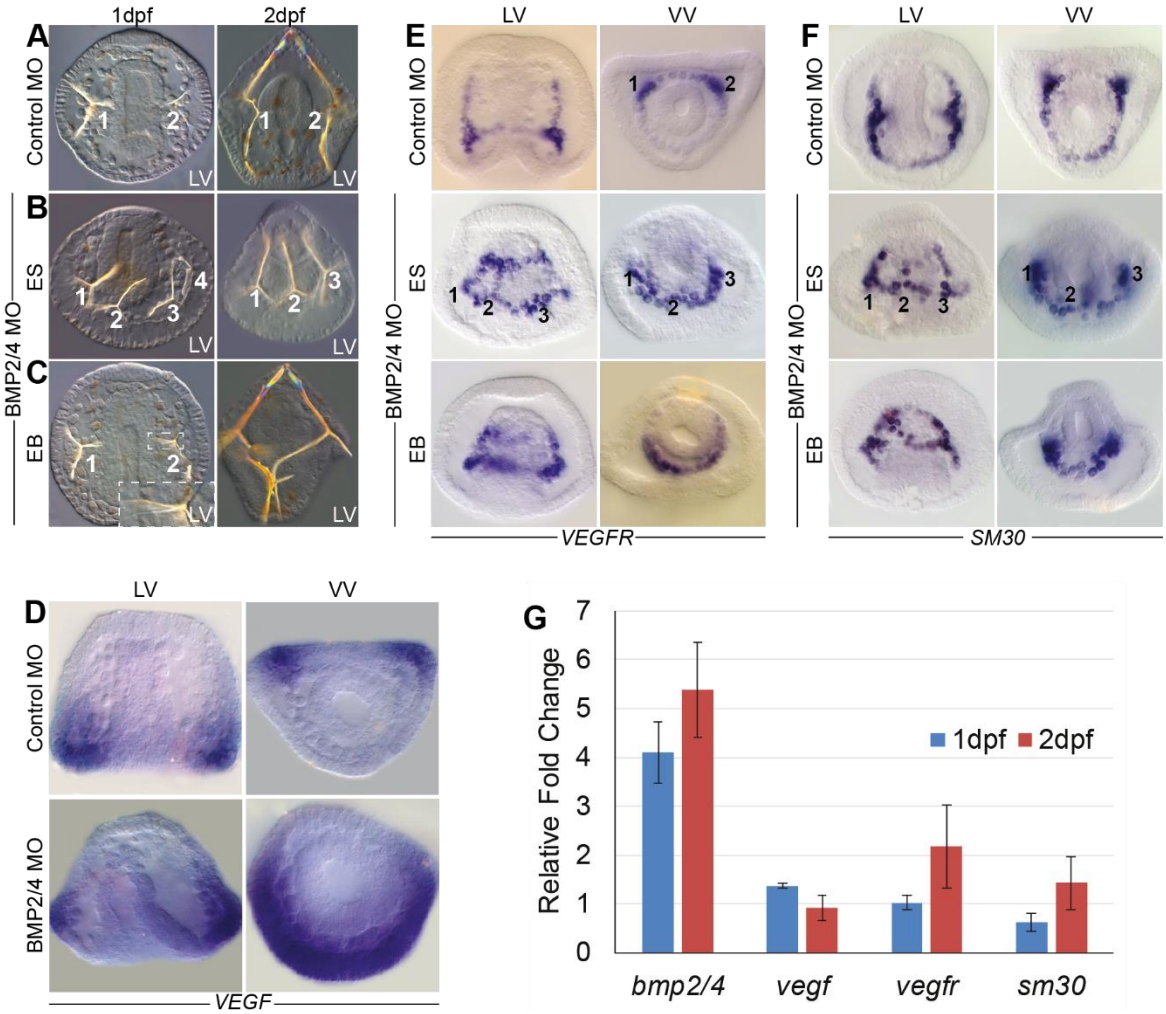

Figure 2 BMP2/4 controls skeletal patterning and VEGF expression. (A) Embryos injected with control MO show normal two spicules at 1dpf (left, 110/110 of scored embryos show this phenotype) and 2dpf (right, 56/56). **(B-C)** BMP2/4 MO injected embryos show either ectopic spicules indicated by numbers (ES, 89/169 1dpf, 120/135 2dpf) or ectopic spicule branching (EB, 39/169 at 1dpf, 15/135 at 2dpf). **(D)** VEGF expression is localized in two lateral patches in control embryo (top) and is strongly expanded in embryos injected with BMP2/4 MO at 1dpf (bottom). **(E-F)** VEGFR and SM30 expression in control embryo (top) and in BMP2/4 morphants (middle and bottom) at 1dpf. BMP2/4 MO leads to the expansion of the expression either into ectopic skeletal cell-clusters indicated by numbers (ES) or to continuous expansion (EB). LV, lateral view, VV, ventral view. Phenotypes are based on ≥3 independent biological replicates and spatial expression were observed in two independent biological replicates where ≥30 embryos were scored in each condition. **(G)** Fold change in gene expression in BMP2/4 MO compared to control MO embryos at 1dpf (blue column) and 2dpf (red column). Fold change of 1 indicates no change in gene expression. The level of *BMP2/4* mRNA increases by BMP2/4 knockdown in agreement with previous studies (Ben-Tabou de-Leon et al., 2013), since the dorsal side is shrinking, and the ventral side is expanding. Error bars indicate standard deviation over two independent biological replicates.

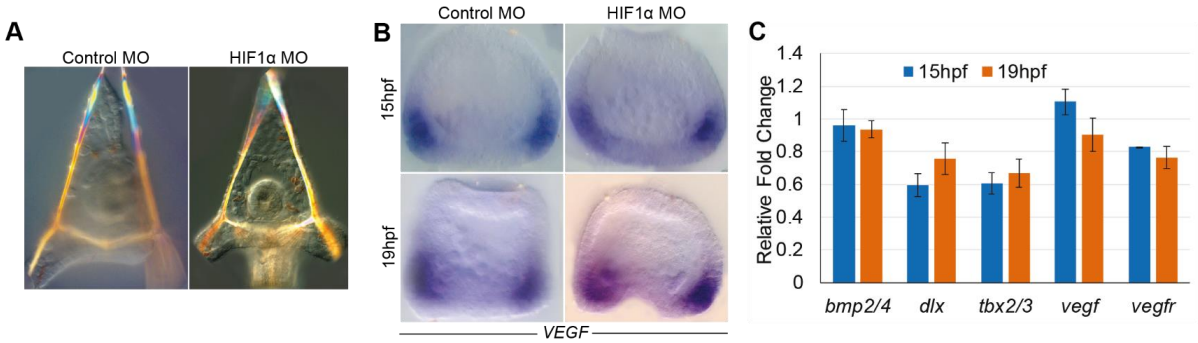

Figure 3 Sea urchin HIF1α does not affect skeletal patterning and VEGF expression. (A) Control (left) and HIF1α MO injected embryos (right) show comparable skeletal structure at 2dpf. **(B)** VEGF expression is similar in embryos injected with control MO (left) and HIF1α MO (right) at 15hpf (top) and 19hpf (bottom). Phenotypes are based on ≥3 independent biological replicates and spatial expression were observed in two independent biological replicates where ≥30 embryos were scored in each condition. **(C)** Fold change in gene expression in HIF1α MO compared to control MO embryos at 15hpf (blue) and 19hpf (orange). Fold change of 1 indicates no change in gene expression. Error bars indicate standard deviation over two independent biological replicates.

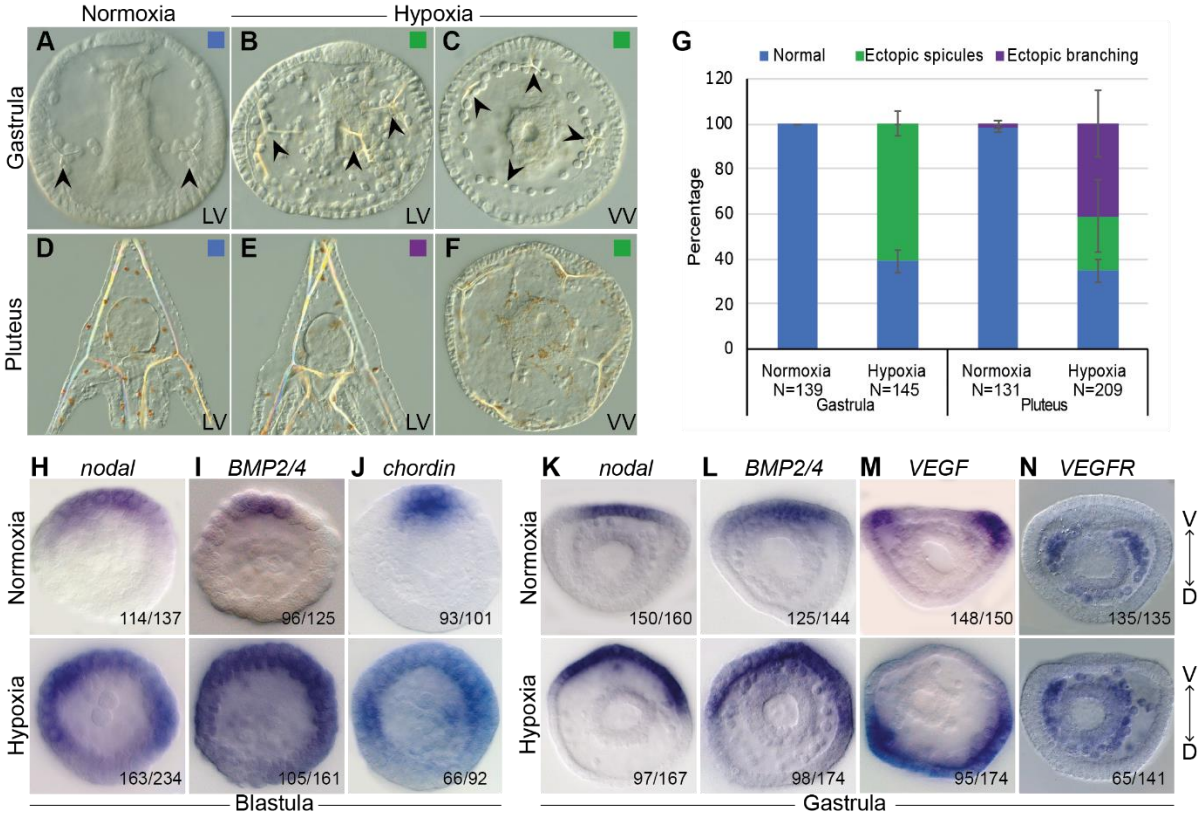

Fig. 4. Growth in hypoxic condition leads to skeletal defects and perturbs the expression of DV and skeletal patterning genes. (A-C) Representative images of embryos at gastrula stage. **(A)** Embryo grown in normoxic conditions shows normal development of two spicules. **(B-C)** embryos grown in hypoxic condition show ectopic spicules, indicated by arrowheads. **(D-F)** Representative images of embryos at pluteus stage. **(D)** Embryo grown in normoxic conditions shows normal skeleton. **(E)** Embryo grown in hypoxic condition shows a normal DV axis and ectopic spicule branches. **(F)** Radialized embryo grown in hypoxic conditions that displays multiple ectopic spicules. LV, lateral view; VV, ventral view. **(G)** Quantification of skeletogenic phenotypes at gastrula stage and pluteus stage. Color code is indicated in the representative images. Error bars indicates standard deviation of three independent biological replicates. **(H-J)** Spatial expression of *nodal*, *BMP/4* and *chordin* genes in normoxic (top) and hypoxic embryos (bottom) at blastula stage. **(K-N)** Spatial expression of *nodal*, *BMP2/4*, *VEGF* and *VEGFR* genes in normoxic (top) and hypoxic embryos (bottom) at the gastrula stage. Embryos are presented in ventral view and the axis is labeled as V, ventral and D. Throughout H-N, the numbers at the bottom right indicate the number of embryos that show this expression pattern out of all embryos scored, based on three independent biological replicates.

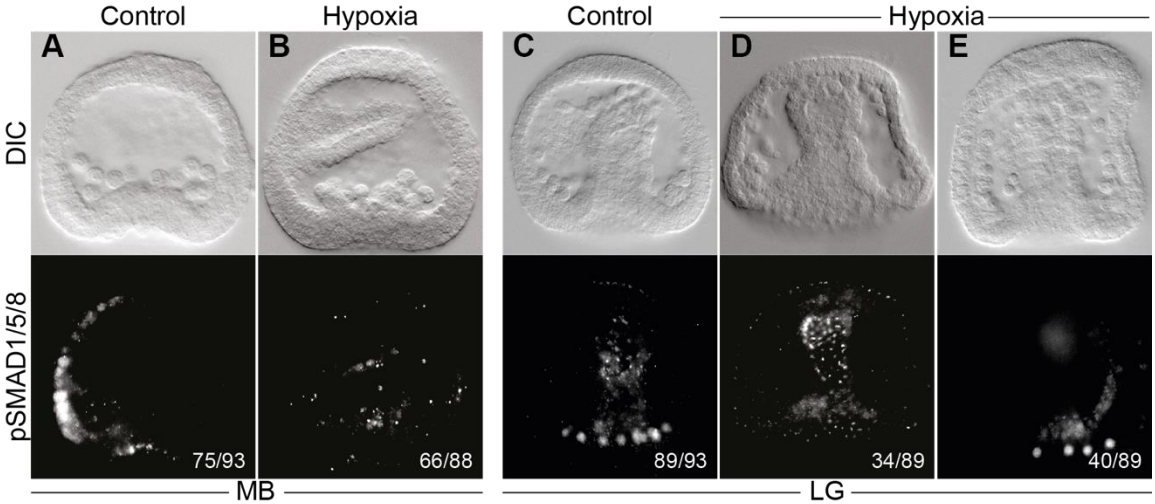

Fig. 5. BMP activity is reduced in hypoxic conditions. (A-B) Nuclear pSMAD1/5/8 patterning in normoxic and hypoxic conditions at mesenchyme blastula (MB) stage. In normoxic conditions, pSMAD1/5/8 staining is detected in the dorsal ectoderm (A), while in hypoxic embryos the signal is completely abolished (B). **(C-E)** pSMAD1/5/8 staining in normoxic vs. hypoxic embryos at late gastrula (LG) stage. pSMAD1/5/8 is detected in the nuclei of the dorsal skeletogenic cells of normoxic embryos (C), while in hypoxic conditions the signal is either not detectable (D) or strongly reduced (E). DIC images of the embryos are presented in the upper row of each panel, and immunostaining of pSMAD1/5/8 of the embryos are presented in the lower row. All embryos are presented in lateral view (LV). The numbers shown on the bottom right of each figure indicate the number of embryos that show this expression pattern out of all embryos scored, based on three independent biological replicates.

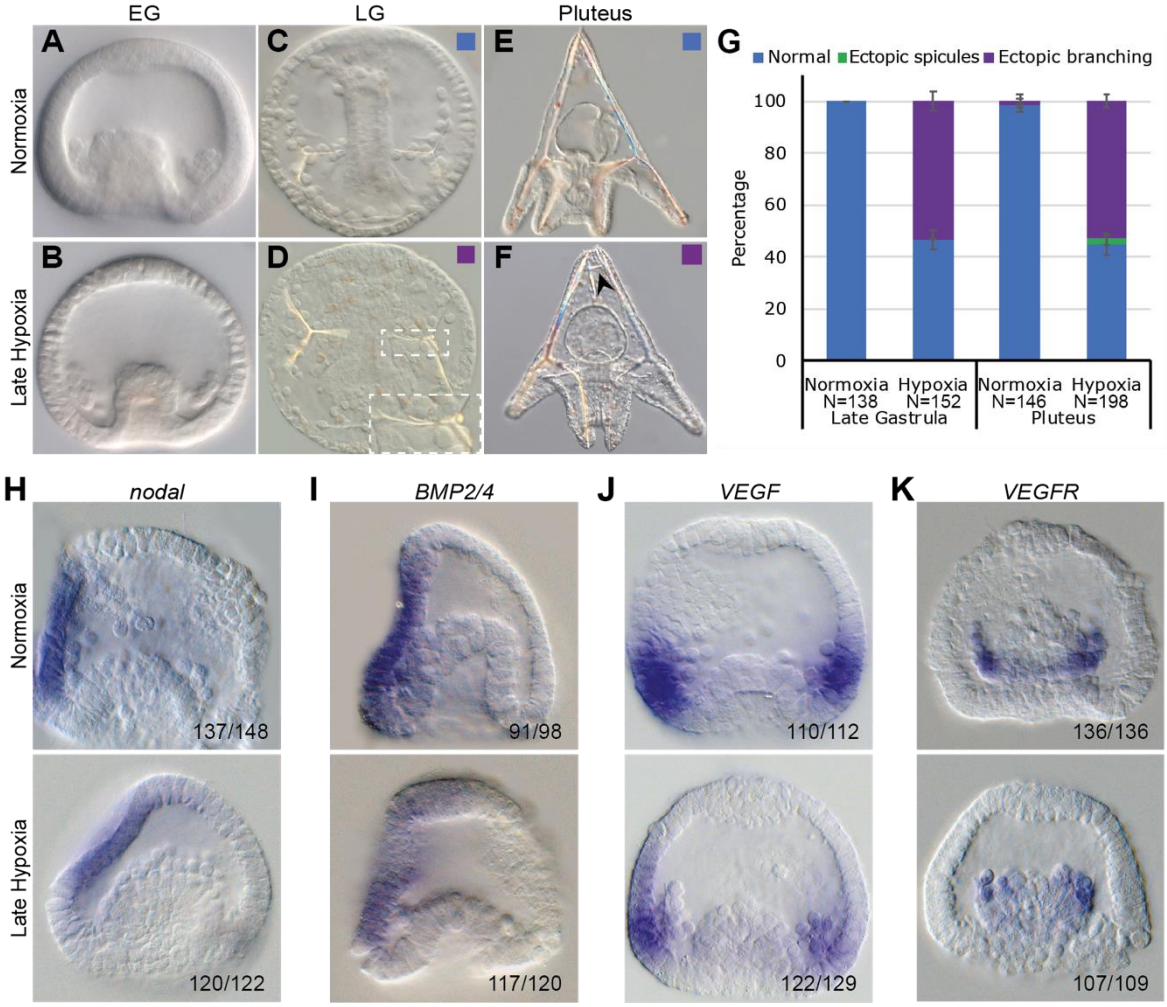

Fig. 6. Late hypoxia affects skeletal structure but not skeletal patterning. (A-F) Images of live embryos, normoxic embryos are presented in the upper row, and equivalently staged hypoxic embryos are on the bottom. **(A-B)** Embryos at early gastrula stage show similar morphology in normoxia and hypoxia. **(C-D)** Hypoxic embryo at late gastrula stage shows two spicules with ectopic spicule branching (D) that are not observed in the normoxic embryo (C). Dashed white square is an enlarged image of the abnormal spicules. **(E-F)** Embryos at pluteus stage. Arrowhead in F, indicates an abnormal spicule growth in the hypoxic embryo. **(G)** Quantification of late hypoxia experiment over three biological replicates. Color code is indicated in the representative images. Error bars indicates standard deviation of three independent biological repeats. **(H-K)** WMISH results of *nodal*, *BMP2/4*, *VEGF* and *VEGFR* at early gastrula stage. Normoxic embryo is presented in the top and hypoxic embryo is in the bottom of each panel. On the bottom right of each figure we indicate the number of embryos that show this expression pattern out of all embryos scored, based on three independent biological replicates.

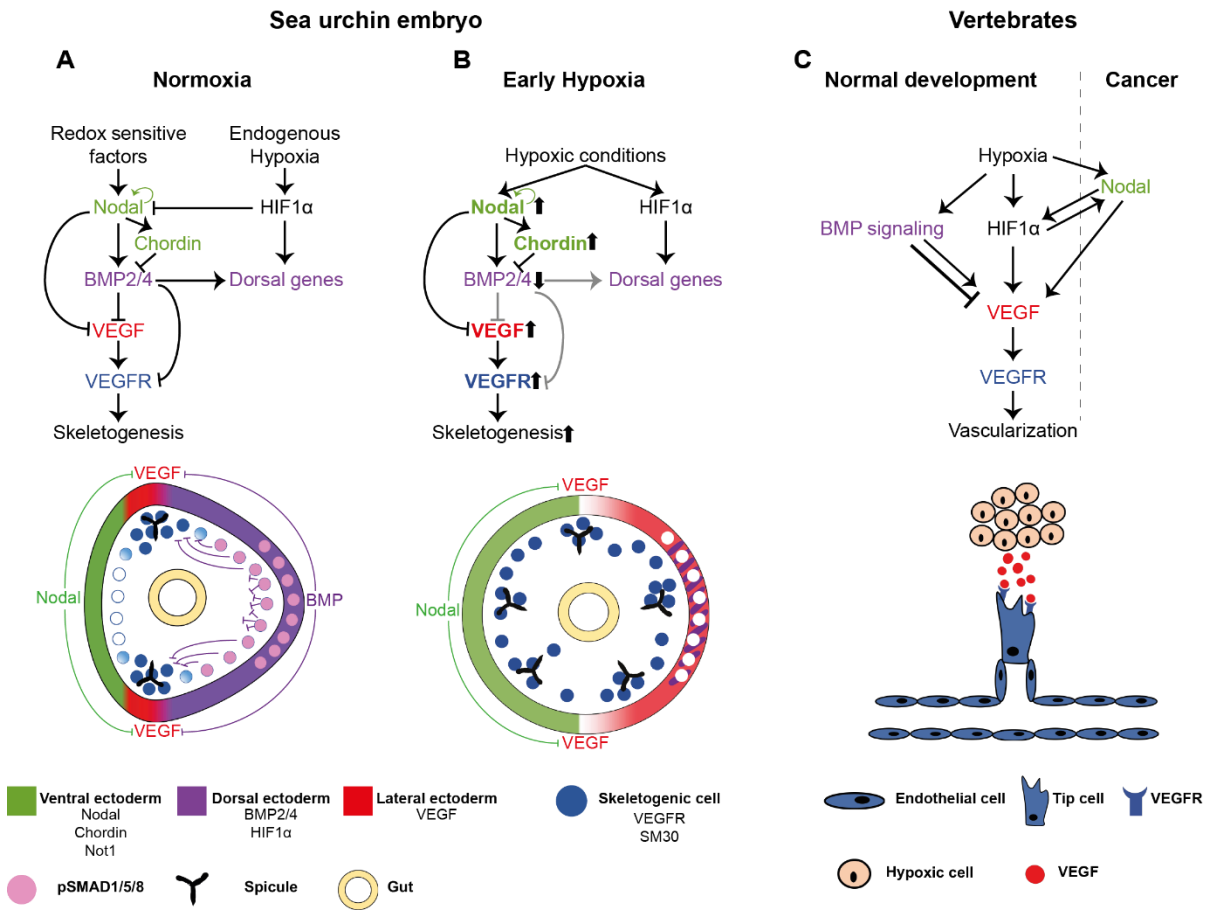

Fig. 7. The interactions between the DV and skeletogenic GRNs, the GRN response to early hypoxia and the similarities to the regulation of vertebrate's vascularization. (A-B) Diagrams showing our proposed model for skeletal patterning in normal conditions **(A)** and Hypoxic conditions **(B)**. Color codes are indicated in the bottom part of the figure. **(A)** During normal development, Nodal represses VEGF expression in the ventral side, Hif1α transiently represses Nodal at the dorsal side and BMP represses VEGF, VEGFR and SM30 expression in the dorsal side. Nodal pathway positively regulates the expression of the *nodal* gene and the activation of BMP inhibitor, Chordin, and by that defines the regulatory states along the DV axis. **B)** Hypoxic conditions applied at early development, expand *nodal* expression and the ventral ectoderm and reduce BMP activity and the dorsal ectoderm. The reduction of BMP activity leads to an expansion of VEGF, VEGFR and SM30 expression in the dorsal side and growth of ectopic skeletal centers. Ascending arrows near a gene name indicate enhanced activity, while descending arrows indicate reduced activity. Gray regulatory links indicate inactive connections under hypoxic conditions. **(C)** Diagram showing a summary of the relevant regulatory interactions during vertebrates' vascularization in normal development and in cancer. In normal development hypoxia regulates HIF1, BMP and VEGF expression to induce vascularization. In cancer cells, hypoxia upregulate Nodal that interacts with HIF1 and VEGF to promote angiogenesis.

Supplementary Materials

Table S1: List of qPCR primers used in this study

Gene Name	Forward primer	Reverse primer
BMP2/4	GTACCGGTCGCATACACAAG	TGTGTCTGTGCTGCTCTGTA
dlx	GGGCATCCTCCAATTTATGA	GCAAGGTATTGGGTCTGGTG
tbx2/3	TATTACCACCTCGCCTCAGC	CCTGGATGTTCGCCGAATTT
VEGF	GCTCATGGTTCTCTCGAAGG	CCCGCTGAGATAACATTGGT
VEGFR	CACTGGGAGATATCGGTGCT	ACGGTTGCCCACGATAAATA
SM30	AGGTGGTTTCCCTGGACAAG	TTGGGCATGTCTCCTGTCTT

Table S2: List of WMISH PCR primers used in this study

Gene Name	Forward primer	Reverse primer
BMP2/4	GTGGCGAAAGAGGAGCGAC	GATGGTTCTGATCAAGAAGTC
nodal	CATCCATCGGAGCAACTCTTC	CAAAGTTCAAAATCGAATCGGC
chordin	GACCATGTACCGTGTCGTGATTTATAC	CCCTGAGCCAAACCATCACGG
VEGFR	GTAACTCATAATCCATGCTAC	GCTACTATTCAATGTCATTTC
SM30	CCTCCCCCTTTCGTGTTATAAATG	GCAAAACAACTTCTTCGTCGGTC